ChemCatChem

Research Article
doi.org/10.1002/cctc.202301632

Chemistry Europe
European Chemical Societies Publishing

www.chemcatchem.org

Transition-metal Substituted Polyoxometalates as Soluble RedOx Mediators in Electrocatalytic Biomass Conversion

Sonja D. Mürtz,[a] Jan-Christian Raabe,[b] Maximilian J. Poller,[b] Regina Palkovits,*[a, c] Jakob Albert,*[b] and Nils Kurig*[a]

Polyoxometalates (POMs) are known for their unique redox properties, making them interesting candidates as redox mediators in electro-organic transformations. We investigated derivatives of $H_3[PMo_{12}O_{40}]$, a classical Keggin-type POM, as a potential redox mediator in the indirect electrolysis of biobased glyceraldehyde (GLAD), focusing on the effects of double substitution of the Mo framework metal by redox active transition metals (Mo replaced by V, Ni, Co, Mn). By combining electrochemical techniques with HPLC, UV-Vis spectroscopy, and ^{31}P-NMR spectroscopy, a comprehensive overview of the reaction pathways, as well as the electronic and structural changes of the POM during the reaction were revealed. This work not only contributes to the fundamental understanding of POMs as redox mediators, but also paves the way for innovative development of sustainable and environmentally friendly electro-organic transformations.

Introduction

In recent decades, polyoxometalates (POMs), also called iso- or heteropolyanions, have emerged as a fascinating class of molecular metal oxides, that have attracted considerable attention in catalysis due to their remarkable structural diversity and high ability to drive various chemical reactions. They consist of different metal-oxygen polyhedra MO_x (mostly octahedra MO_6).[1–7] Formally, POMs are oxo complexes in which the oxo ligands coordinate the metals in a terminal M=O and bridging M–O–M bond motif. Normally, POMs are formed with group five and six metals such as tungsten W, molybdenum Mo, vanadium V, niobium Nb, and tantalum Ta in their highest oxidation states.[4,8] The MO_6 octahedra can be linked via shared edges and corners. Several different POM structure-types are known, resulting from the different geometrical connection motifs of the polyhedra. A possibility to form a POM structure is to involve different main group element polyhedra XO_n. Those elements are then called heteroatoms (X) in the context of POM chemistry. The resulting structural motifs are then called heteropolyanions or heteropolyacids (HPAs).[8] Prominent examples are the Keggin structure[4,7,9–13] with the general molecular formula $[XM_{12}O_{40}]^{n-}$ (e.g. $[PW_{12}O_{40}]^{3-}$ and $[PMo_{12}O_{40}]^{3-}$), the Wells-Dawson-structure[9,14–16] $[X_2M_{18}O_{62}]^{n-}$ (e.g. $[P_2W_{18}O_{62}]^{6-}$), and the Anderson-Evans structure $[XM_6O_{24}]^{n-}$ (e.g. $[TeMo_6O_{24}]^{6-}$ or $[TeW_6O_{24}]^{6-}$).[17,18] Key properties of these clusters are a high water solubility, especially of the protonated form, as well as the ability to reversibly receive and donate multiple electrons and protons normally through outer-sphere mechanisms.[19,20] Weinstock *et al.*[20] provided an explanation that the electron transfer is a so-called outer-sphere mechanism. According to this, POMs have charge densities that are lower than those in classical anions such as PO_4^{3-}, NO^{3-} etc. and the negative charge densities on the terminal M=O ligands are lower than those of the bridging M–O–M ligands. In addition, all metal atoms are coordinatively saturated, limiting their direct coordination to electron donors and acceptors.[20] These properties can be used in oxidation or hydrogenation of various organic compounds.[17,21–23] Applications include analytical chemistry and catalysis, but also biochemistry, medicine, geochemistry, as well as material sciences.[3,24,25]

The well-understood redox properties render POMs of particular interest as inorganic molecular redox mediators for electro-organic transformations which remained a rather niche area in research up to now.[26–31] In an indirect electrolysis, redox mediators act as electron transfer agents between the electrode and the substrate in solution. For example, the mediator is oxidized at the anode surface and diffuses into the bulk solution where it is reduced by an organic substrate before returning to the anode to be oxidized again. The oxidized substrate can then undergo subsequent chemical reactions in the solution.[32] Hence, the heterogenous step of the electron transfer to the species in solution is decoupled. The chemistry at the phase boundary occurs only between the electrode and

[a] S. D. Mürtz, Prof. Dr. R. Palkovits, Dr. N. Kurig
Institute for Technical and Macromolecular Chemistry
RWTH Aachen University
Worringerweg 2, 52074 Aachen, Germany
E-mail: palkovits@itmc.rwth-aachen.de
kurig@itmc.rwth-aachen.de

[b] J.-C. Raabe, Dr. M. J. Poller, Prof. Dr. J. Albert
Institute for Technical and Macromolecular Chemistry
University of Hamburg
Bundesstr. 45, 20146 Hamburg, Germany
E-mail: jakob.albert@uni-hamburg.de

[c] Prof. Dr. R. Palkovits
Institute for Sustainable Hydrogen Economy (INW-2),
Forschungszentrum Jülich,
Am Brainergy Park 4, 52428 Jülich, Germany.

Supporting information for this article is available on the WWW under https://doi.org/10.1002/cctc.202301632

the ideally robust and recyclable redox mediator, which can be a great advantage preventing uncontrolled oxidation or reduction that leads to polymerization or degradation of the substrate.[33] The redox mediator might also have lower electron transfer barriers with the electrode than the substrates themselves and could bypass the slow kinetics of direct electrolysis, leading to a decreased overpotential.[34] Usually, simple metal salts or small organic molecules are used as redox mediators, so POMs could play a complementary role here due to their wide variety of structures and properties.[35]

Until 2010, very little work on POMs as redox mediators has been done as first approaches in 1990 reported very slow reaction rates.[36–38] Firstly, POMs were implemented as redox mediators in batteries[39] and fuel cell applications.[40–43] In the field of organic transformations, Neumann *et al.*[44] reported the conversion of methylarenes using $H_5[PV_2Mo_{10}O_{40}]$ oxidized at the anode together with H_2 production at the cathode. Five cycles were demonstrated, and a mechanism was proposed.[44,45] Regarding non-aromatic substrates, the oxidation of light alcohols mediated by $[\{Ru_4O_4(OH)_2(H_2O)_4\}(\gamma\text{-}SiW_{10}O_{36})_2]^{10-}$(1[(γ-$SiW_{10}O_{36})_2]^{10-}$) was reported by Liu *et al.*,[46] as well as the oxidation of light hydrocarbons using$\{Fe_{30}W_{72}\}$ by Neumann.[47] Recently, Stergiou and Symes published their studies on selective electrocatalytic reduction of substituted nitrobenzenes to their aniline derivates using $H_3[PW_{12}O_{40}]$ as a redox mediator.[48–50] Although POMs represent an important catalyst class for biomass conversion,[4] electrochemical applications in this field are rare.[51,52] Electrochemical biomass conversion is considered an important 21st century technique because it combines renewable carbon feedstocks and decarbonized electrical energy.[53–56]

In this contribution, we investigated Keggin-type POMs based on $H_3[PMo_{12}O_{40}]$ as redox mediators in the indirect electrolysis of bio-based glyceraldehyde (GLAD), focusing on the effect of double foreign transition metal substitution (Mo replaced with V, Ni, Co, Mn) in the Keggin-phosphomolybdate structure.[57] The choice was on the substituted phosphomolybdate structures, since we were able to show in a previous study that the redox chemistry of the corresponding phosphotungstate structures is significantly less pronounced than that of the molybdates. So the molybdates prove to be more promising candidates for redox catalytic applications.[7] By systematically studying their distinct performances, we aim to shed light on the potential of these POMs as promising electrocatalysts in green oxidation processes. Using a combination of analytical techniques such as HPLC, UV-Vis spectroscopy, and ^{31}P-NMR spectroscopy, we investigated the mechanisms of the underlying catalytic transformations, as well as the active species and characterized the reaction products. This work enhances the fundamental understanding of POMs as redox mediators and contributes to the development of sustainable and environmentally friendly electro-organic transformations with potential applications in the field of green chemistry.

Results and Discussion

In order to investigate the performance of Keggin-type POMs as redox mediators in the electrocatalytic oxidation of bio-based substrates and the influence of foreign metal substitution, we tested five different POMs: the unsubstituted $H_3[PMo_{12}O_{40}]$ (HPMo) and different double foreign element substituted derivatives such as $H_5[PV_2Mo_{10}O_{40}]$ (HPV_2Mo), $H_{11}[PNi_2Mo_{10}O_{40}]$ ($HPNi_2Mo$), $H_{11}[PCo_2Mo_{10}O_{40}]$ ($HPCo_2Mo$), and $H_{11}[PMn_2Mo_{10}O_{40}]$ ($HPMn_2Mo$). All POMs used in this work were analyzed regarding their stoichiometry by inductively coupled plasma optical emission spectroscopy (ICP-OES) and the amount of hydration water was determined using thermogravimetric analysis (TGA) as shown in Figures S1 and S2. From the TGA curves, a significant mass loss can be seen when the samples are heated to 350 °C, which correlates to the evaporation of the hydration water. In the last phase, in which the temperature is constant at 350 °C, a constant mass is achieved, the mass which represents the dried POM material. The results confirmed the desired stoichiometry and are summarized in Tables S1–S4 in the ESI. The integrity of the Keggin-structure was verified using vibrational spectroscopy (ATR-FT-IR and Raman) as shown in Figures S3 and S4. Additional characterization in aqueous solution was performed by ^{31}P and ^{51}V-NMR analysis (Figures S5 and S6) as well as UV-Vis spectroscopy (Figure S7) to study the dissociation behavior of the POMs in aqueous solution. Using Lambert-Beer's law the extinction coefficients were determined and summarized in Table S5 (see Figures S8 to S13).

For electrocatalytic applications, the redox potentials play a crucial role, and therefore, were analyzed using cyclic voltammetry (CV) and square-wave-voltammetry (SWV) as shown in Figure 1. The comparison between the unsubstituted POM and the substituted POMs reveals a number of interesting differences in the redox potentials: V(V) produces additional reduction peaks while Ni (II) does not significantly influence the redox

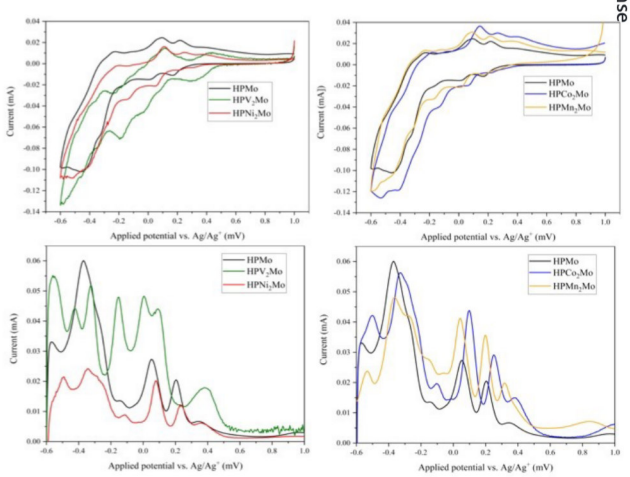

Figure 1. CV data (top left and right) of all investigated POM structures in comparison with the unsubstituted Keggin-type structure HPMo. Additionally, SWV measurements (bottom left and right) were performed to highlight the differences in the electrochemical data of the different POMs. All measurements were performed in aqueous solution at pH 1 (1 mmol/L). 0.1 M hydrochloric acid was used as supporting electrolyte.

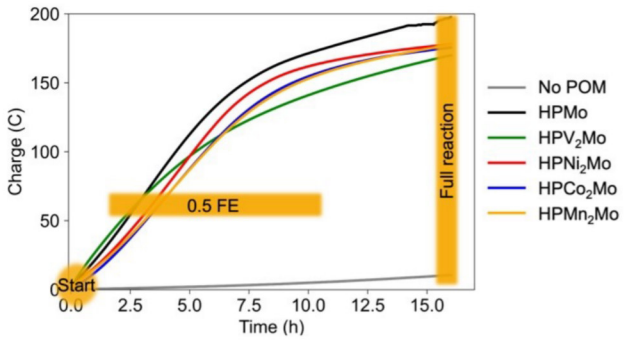

Figure 2. Overview of integrated transferred charges in the electrocatalytic GLAD oxidation mediated by the unsubstituted parent POM (HPMo) as well as the double-substituted POMs. Conditions: Pt anode, Pt cathode, 1.2 V vs RHE, 0.1M GLAD, 30 mg/mL POM, 0.1 M HCl, T = 80 °C.

behavior, whereas Co(II) and Mn(II) shift the potentials to higher values.[6] Overall, the CV and SWV data of the POMs used here show that foreign metal substitution significantly shifts the redox potentials of the resulting transition-metal substituted POMs, which makes the selected POMs interesting for using them as mediators for the electrocatalytic oxidation of organic substrates. The observed differences in the electrochemical data can be attributed to the different electronic structures of the POMs, which result when one or more elements in the Keggin structure are substituted with foreign elements.

Glyceraldehyde (GLAD) was selected as a bio-based substrate for this study through a substrate screening process (for details see Figure S16). The reaction was conducted using a divided three-electrode batch cell (Figure S14) with platinum electrodes at 1.0 V *vs.* Ag/AgCl 3 M KCl (pH = 0, 1.2 V *vs.* RHE), and the reaction solution was preheated at 80 °C for 0.5 hours to initiate the oxidation reaction and the reduction of the POMs (Figure S15). The POM as a redox mediator was then oxidized at the anode during electrolysis and reduced by GLAD in solution, simultaneously hydrogen evolution took place at the cathode. A blank experiment using the Pt anode without addition of POM showed no conversion of the organic substrate under the given reaction conditions. Figure 2 provides an overview of the performance of the various POMs, showing the charges transferred over time.

The figure highlights three critical stages of the reaction, which will be discussed in more detail below. The beginning of the electrolysis after preheating the reaction solution is the first point. As the reaction progresses, the second point is reached at 0.5 Faraday equivalents (FE) referred to a two-electron oxidation of GLAD. This corresponds to a transferred charge for a theoretical conversion of GLAD to glyceric acid (GLA) of 50%. After about ten hours, a decreased slope in the integrated charge over time graph can be observed. Here, the substrate is depleted, and the POM is oxidized until almost no charge is transferred at the end of the reaction after 16 hours (third point). This point is referred to as "full reaction" because POM and substrate are both fully oxidized. The reaction temperature was set to 80 °C to enable the thermal reaction between the substrate and the POM.

The initial current density plays a crucial role in determining the performance as it is directly related to the oxidizing abilities and electrochemical behavior. Therefore, the current density using the different POMs was analyzed at those three points of the reaction process, which is depicted in Figure 3. Here, it becomes evident that HPMo itself is already well-suited as a redox mediator for GLAD oxidation, and the substitution with V(V) has a very positive impact, while the current density remains the same for Ni(II), Co(II), and Mn(II). This can be explained by looking at the trend from the electrochemical characterization above, which showed that V(V) shifts the redox potentials to the lowest values, which results in the highest activity. While applying the same potential for all POMs during electrolysis, the lower redox potentials have a positive impact, because it means a larger overpotential applied. In the middle of the reaction, after 0.5 FE to GLA, the differences become negligible, the POMs reach similar current densities at this stage of the reaction, albeit after different times. It is important to note here that this comparison is made at a point where equal amounts of charge were transferred to the solutions. In the case

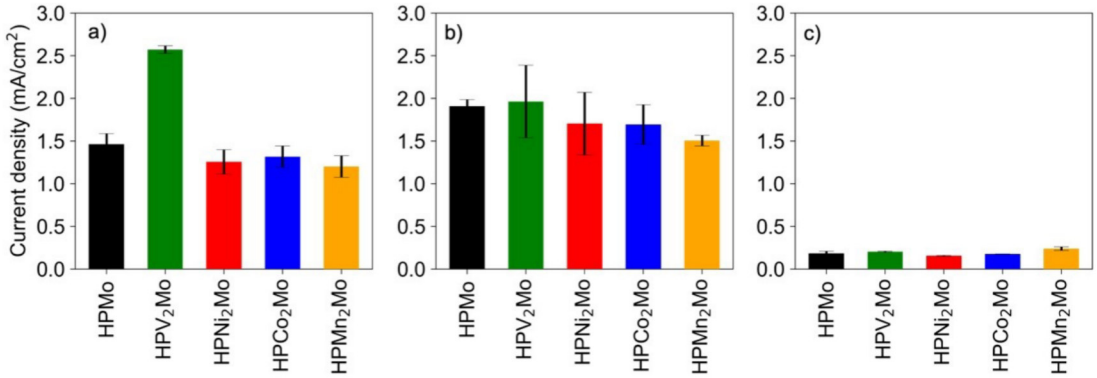

Figure 3. Current densities of the electrocatalytic GLAD oxidation mediated by the unsubstituted parent POM (HPMo) as well as the double-substituted POMs after a) one hour of electrolysis, b) 0.5 FE, and c) 16 h of electrolysis. Conditions: Pt anode, Pt cathode, 1.2 V vs RHE, 0.1M GLAD, 30 mg/mL POM, 0.1 M HCl, T = 80 °C.

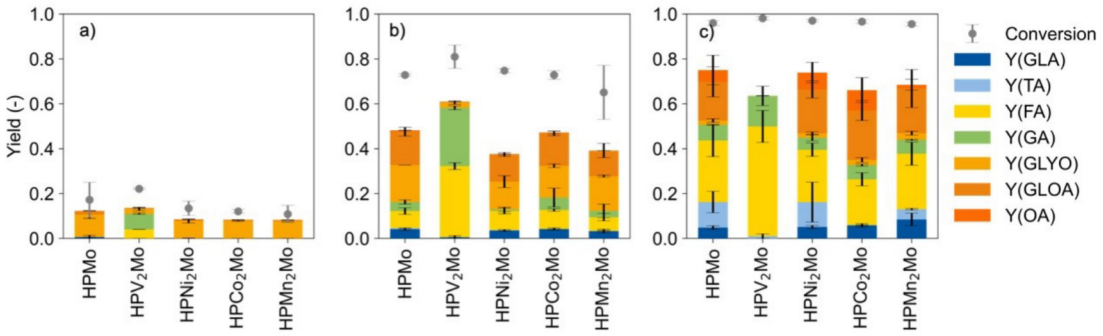

Figure 4. Product formation in the electrocatalytic GLAD oxidation mediated by the unsubstituted parent POM (HPMo) as well as the double-substituted POMs after a) preheated reaction solution (0.5 h at 80 °C) before electrolysis, b) 0.5 FE, and c) 16 h of electrolysis. Conditions: Pt anode, Pt cathode, 1.2 V vs RHE, 0.1M GLAD, 30 mg/mL POM, 0.1M HCl, T = 80 °C.

of HPV_2Mo, more substrate was converted up to this point as it is more efficient. The now decreased substrate concentration causes a lower current density compared to the other reaction systems. After 16 hours at the end of the reaction, the current density tends to zero as no substrate is left, and the POMs are already fully re-oxidized. The product spectrum was analyzed using high-performance liquid chromatography (HPLC), and the results are presented in Figure 4. The liquid phase contained various products, including glyceric acid (GLA), tartronic acid (TA), formic acid (FA), glycolic acid (GA), glyoxal (GLYO), glyoxalic acid (GLOA), and oxalic acid (OA), which were quantified using the methods described in Tables S6 and S7. Preheating of the reaction solution initiated the chemical reaction, oxidizing GLAD, while simultaneously reducing the POM. The completion of this reaction was also visible to the eye, as the color of the solution changed from yellow to dark blue. The conversion ranged from 10 to 20%, primarily yielding GLYO for HPMo, $HPNi_2Mo$, $HPCo_2Mo$, and $HPMn_2Mo$. This correlates well with a stoichiometry of approximately one to five, POM versus GLAD, in the solution. In contrast, HPV_2Mo yielded more GA and FA, suggesting different oxidation pathways. After 0.5 FE, the conversion increased by 50–60%, and a distinct oxidation pathway for HPV_2Mo, compared to the HPMo, $HPNi_2Mo$, $HPCo_2Mo$, and $HPMn_2Mo$, became evident. Notably, mainly FA and GA are formed with yields of GLYO and GLOA lower than 5%. Based on these findings, we propose the following reaction scheme (Scheme 1).

The aldehyde group of GLAD undergoes oxidation to form GLA, and further oxidation may occur on the terminal hydroxy group, leading to TA. However, this reaction does not appear to be favoured here, as TA is only observed at the end of the reaction in low amounts. The POMs catalyze C–C bond cleavage in this reaction, resulting in formic acid and C_2-products. For the reaction using HPV_2Mo, mainly FA and GA are observed at all stages of reaction progress, indicating a C–C cleavage reaction and subsequent oxidation to GA. Interestingly, glycolaldehyde was not observed, as it seems unstable under these reaction conditions and forms GA immediately. Additionally, further oxidation of GA was not observed using the V-substituted POM. The third pathway involves oxidative C–C cleavage leading to

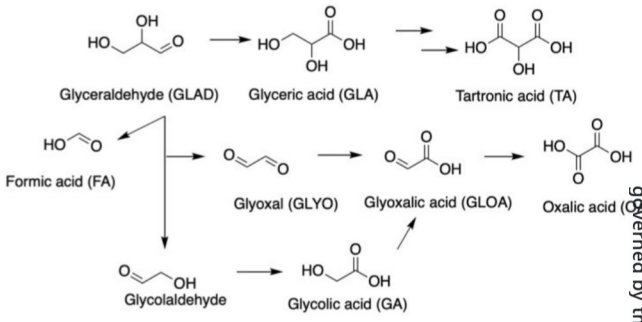

Scheme 1. Proposed reaction pathways of Keggin-type POM mediated electrolysis of GLAD.

GLYO and further to GLOA and OA, which was observed for HPMo, $HPNi_2Mo$, $HPCo_2Mo$, and $HPMn_2Mo$. Substitution by various transition metals also had an influence on the selectivity of the reaction within this pathway as well. The oxidation of GLA to TA was favoured on HPMo and $HPNi_2Mo$ while further oxidation is decreased for $HPMn_2Mo$ and does not take place for $HPCo_2Mo$. Only small amounts of OA were observable at the end of the reaction indicating that this is not the final product. We assume it partly decomposes into gaseous products, such as CO_2, which also explains the discrepancy in the mass balance of around 20%.[58] In order to derive more information on mechanisms and active species of the reactions, the state and electronic properties of the POMs were characterized using UV-Vis spectroscopy (Figure 5). The HOMO-LUMO (HOMO = highest occupied molecular orbital, LUMO = lowest unoccupied molecular orbital) excitation of substituted phosphomolybdates typically involves a Ligand-to-Metal-Charge-Transfer (LMCT) transition, leading to intense bands in the UV-Vis spectra. The position of these bands depends on the oxidation state and type of transition metal present.[4,6] Before the reaction, the UV-Vis spectra of the reaction solutions show this LMCT band at 294 nm for HPMo, $HPNi_2Mo$, $HPCo_2Mo$, and $HPMn_2Mo$, which can be assigned to the $O \rightarrow Mo^{VI}$ LMCT (transition of an electron from the oxo ligand to the molybdenum atom). The spectra of HPV_2Mo before the reaction shows a maximum at 309 nm, which relates to the V(V) LMCT, while the Mo(VI) LMCT is visible

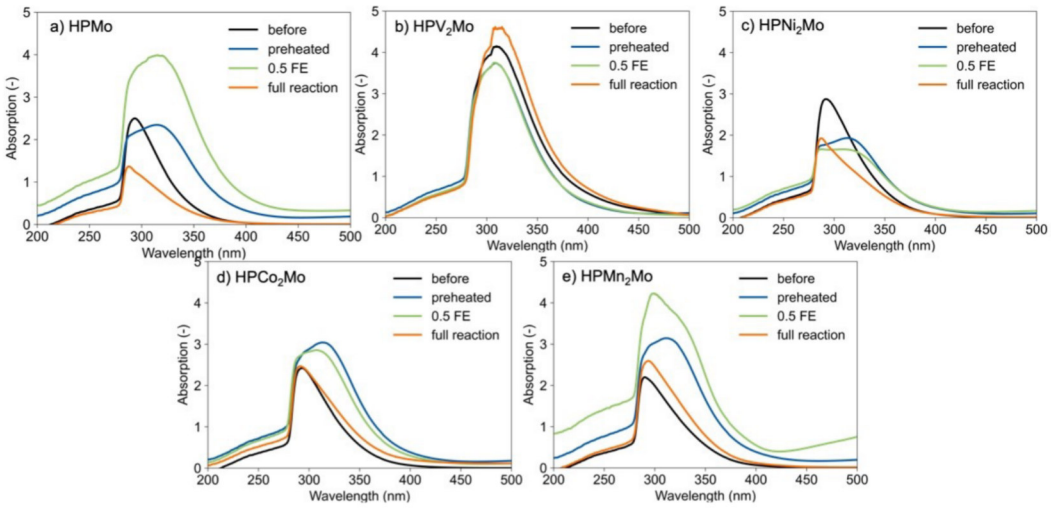

Figure 5. UV-Vis spectra of the reaction solution before the reaction, after preheating, at 0.5 FE and after 16 hours of electrocatalytic GLAD oxidation mediated by a) HPMo, b) HPV_2Mo, c) $HPNi_2Mo$, d) $HPCo_2Mo$, e) $HPMn_2Mo$. Reaction solution was diluted 1:80 with distilled water.

as a shoulder to the left. LMCTs for the other substituted metals are not visible, because transitions between the metals d-orbitals with their spin configurations are forbidden, so that there is no room for an LMCT excitation. However, after the pretreatment and during electrolysis, reduced species become evident as a red-shifted shoulder in the spectrum, noticeable for HPMo, $HPNi_2Mo$, $HPCo_2Mo$, and $HPMn_2Mo$. This could indicate a change in the electronics of the molybdenum species. The POM is reduced by the reaction with the organic substrate, lowering all energy levels. So, less energy is needed for exciting the corresponding LMCT, resulting in a shift of the LMCT bands to higher wavelengths. However, this is not visible for HPV_2Mo. V(V) substituted phosphomolybdates are known to form pervanadyl cations VO_2^+ in aqueous solution. The formation of free VO_2^+ cations by solvated, V(V) substituted Keggin POMs has already been discussed in the literature and can be observed for example in the ^{51}V NMR spectra by a broad peak at a chemical shift of −545 ppm.[4] During the reaction the VO_2^+ cations are reduced to vanadyl cations VO^{2+}. Afterwards, the electrons are not located in the Mo orbitals, which means that the UV-Vis spectra after reduction remain unchanged.[58–60] At the end of the reaction, the spectra prove reoxidizability to the original state of the POMs as the shoulder disappears again. The characteristics of the POMs during the reaction were further investigated by ^{31}P-NMR (Figure 6). A comparison of the POM state before the reaction with the spectra obtained after preheating and during the electrolysis revealed distinct structural and especially electronic changes related to the reduction of the POMs. The reduced POMs contain unpaired electrons and become paramagnetic as indicated by broadening of the peaks. Generally, the spectra after the completed reaction resembled the state before the reaction, indicating again successful reoxidation. The HPV_2Mo stands out, showing several signals of structural isomers around −4.1 ppm (Figure 6 b) indicating a redistribution of V. Due to different conditions in the POM synthesis compared to the catalytic system, different ratios of the structural isomers are obtained before and after the reaction. The observed high mobility of V supports the reaction mechanism via dissociated VO_2^+/VO^{2+}. For all other POMs investigated, minimal changes in the distribution of structural isomers are present after the reaction indicated by additional signals at 4.5 ppm (Fig 6 a,c–e). These compounds also show high similarity during the reaction, which explains the observed catalytic behaviour. A general upfield shift can be explained by the reduced state of the POMs leading to increased shielding. For the $HPMn_2Mo$, decreased signal-to-noise ratio (S/N) can be observed compared to the other POMs, but not related to the oxidation state in the course of the reaction. The as-synthesized $HPMn_2Mo$ is in paramagnetic d^5 configuration, accounting for peak broadening and decreased S/N. Interestingly, this does not change during the reaction, indicating strong charge distribution all over the POM molecule. This is further evidence of the strong similarity of the catalytic activity of all materials except HPV_2Mo. The latter, in turn, shows a greater similarity in the reduced form compared to the oxidized one with respect to the other POMs. Accordingly, the POM species present during catalysis resembles the non-substituted one. We attribute the redox activity of all POMs except HPV_2Mo to the Mo centers explaining their similar reaction pathways. The substituted transition metals are present in oxidation state +II and influence the POMs redox potentials (see Figure 1). In the case of HPV_2Mo, however, the redox chemistry seems to be dominated by V(V). For this POM species, the ability to dissociate to VO_2^+/VO^{2+} appears to be important. The smaller size and higher mobility of VO_2^+/VO^{2+} compared to the parent HPV_2Mo lead to higher activity but a different reaction pathway. Therefore, especially for the i-t course (Figure S18), the results do not correspond to those of the unsubstituted POM, although a comparable species is present due to the V-dissociation (Figure S20). Control experiments using $VOSO_4$ as a VO^{2+} source confirmed that the VO^{2+}/VO_2^+ redox couple plays and important role in the reaction showing

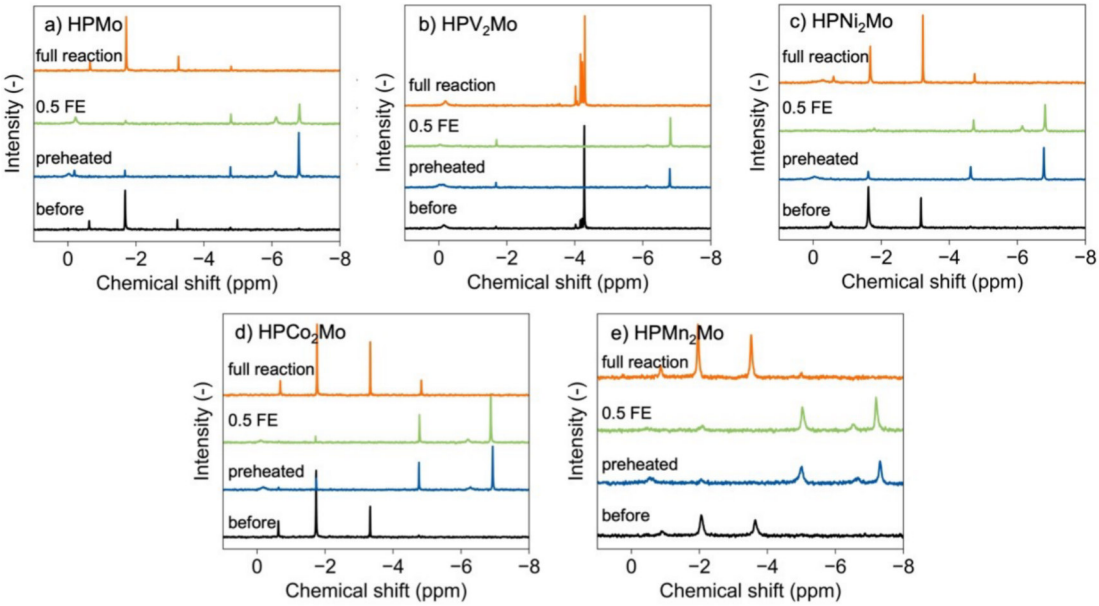

Figure 6. ^{31}P-NMR spectra of the POMs a) HPMo, b) HPV_2Mo, c) $HPNi_2Mo$, d) $HPCo_2Mo$, and e) $HPMn_2Mo$, before the reaction, after preheating, at 0.5 FE and after 16 hours of electrocatalytic GLAD oxidation. The spectra were measured at 162 MHz and 10 v% D_2O was added to the reaction solution.

similar results to HPV_2Mo (Figure S21). It has to be mentioned here that VO_2^+ as the active species cannot be formed thermocatalytically from $VOSO_4$. This is only possible within the POM structure which can also be easily separated for recycling.[61] In addition, the POM structure plays an important role in hindering overoxidation as VO_2^+ alone results mainly in C1 products for higher conversions (Figure S21).

Finally, the reoxidizability and stability of the POMs were confirmed in a fed-batch experiment using HPV_2Mo as the best performer. Therefore, GLAD was added to the anode compartment after the reaction for two more times. All three runs showed the same performance regarding the characteristics of the electrolysis and the product formation (for details see Figure S19). This observation shows the feasibility of a semi-batch approach which could be interesting for future studies on the overall technical potential.

Conclusions

In this study, we showed that $H_3[PMo_{12}O_{40}]$ is very suitable as a redox mediator for the indirect electrolysis of biobased GLAD. By analyzing the effects of double substitution of the Mo framework metal by redox active transition metals, a strong, positive effect of V(V) was revealed, which increased the number and shifts of the redox potentials and thus enhanced electrolysis performance. Substitution by Ni(II), Co(II), and Mn(II) changed the electrochemical properties and selectivity as well. By combining electrochemical techniques with HPLC, we were able to reveal different reaction pathways that also depend on the transition metal substitution showing the C–C bond breaking ability of the POMs. Analysis of the POMs during the reaction using UV-Vis spectroscopy and ^{31}P-NMR spectroscopy showed reversible shifts in the LMCT bands and changes in the structure of the POMs due to the dynamic evolution of the electronic states of the POMs over the course of the reaction, demonstrating especially their re-oxidizability. For HPV_2Mo, the analysis has identified the crucial role played by VO^{2+}/VO_2^+ in conjunction with the POM structure, contributing to its enhanced activity due to its higher mobility and reduced size. Together with the results of the fed-batch experiments, we demonstrated high stability and thus, the suitability of the POMs also in long-term electrolysis.

In conclusion, this study shows the successful implementation of $H_3[PMo_{12}O_{40}]$ as well as HPV_2Mo as redox mediators in an indirect electrolysis of bio-based GLAD and provides insights on the effects of double foreign metal substitution regarding activity, mechanism, and active species. These results could be transferred to other POMs and organics to extend sustainable and environmentally friendly synthesis routes of organic compounds via mediated electro-synthesis.

Experimental

All reagents and substrates obtained commercially were used as received without further purification. The POMs $H_3[PMo_{12}O_{40}]$, $H_5[PV_2Mo_{10}O_{40}]$, $H_{11}[PNi_2Mo_{10}O_{40}]$, and $H_{11}[PCo_2Mo_{10}O_{40}]$, were synthesized according to a modified literature procedure of Odyakov *et al.*[6,62–64] Compound $HPMn_2Mo$ was synthesized according to our previous published procedure.[6] The details of synthesis and characterization of the POMs are summarized in the ESI. Electrolysis experiments were performed in custom-built batch cells (Figure S14) connected to a potentiostat (Metrohm PGSTAT 204 with Nova 2.6). Platinum was used as cathode and anode, Ag/AgCl 3M KCl was the reference electrode. Anode and cathode chamber were

separated by a Nafion®N-324 membrane (0.15 mm thick, Teflon fabric reinforced). The reaction solution in the anode chamber consisted of 0.1 M GLAD in 0.1 M HCl with 30 mg/mL POM and the cathode chamber was filled with 0.1 M HCl. The reaction solution was preheated for 0.5 h at a temperature of 80 °C. Electrolysis was performed at 1.2 V vs RHE at 80 °C as well. Product formation was analysed using HPLC (Shimadzu Prominence LC-20 system). Two methods were used to separate and quantify all oxidation products (ESI Tables S8 and S9). The reaction solution at different stages of the reaction was also investigated using UV-Vis spectroscopy (UV-2600i Shimadzu). Therefore, the sample was diluted 1:80 with MilliQ water which was used as a reference. For ^{31}P-NMR spectroscopy 0.05 mL D_2O were added to 0.45 mL sample. The ^{31}P-NMR spectra were measured in a range of 198 to −198 ppm with an excitation frequency of 161.99 MHz in Bruker Avance spectrometer (9.4 T) at 293 K in 5 mm NMR-tubes.

Acknowledgements

We thank the analytical services from the chemistry department of the Hamburg University, especially the central elemental analysis service around Dr. Dirk Eifler, the NMR-service around Dr. Thomas Hackl, Ute Gralla for measuring numerous Raman samples and Thomas Marx from the research group of Prof. Dr. Peter Burger for lending the equipment and assisting with electrochemical measurements. Part of this work was supported by the Cluster of Excellence Fuel Science Center (EXC 2186, ID: 390919832) funded by the Excellence Initiative by the German federal and state governments to promote science and research at German universities. We also acknowledge funding by the Federal Ministry of Food and Agriculture granted by the Agency for Renewable Resources (FNR, 2220NR101X). S. D. Mürtz thanks Cusanuswerk e.V. for funding. Open Access funding enabled and organized by Projekt DEAL.

Conflict of Interests

The authors declare no conflict of interest.

Data Availability Statement

The data that support the findings of this study are openly available in Zenodo at https://doi.org/10.5281/zenodo.10636450, reference number 10636450.

Keywords: Polyoxometalate · Redox mediator · Indirect electrolysis · Electrosynthesis · Biomass

[1] D. L. Long, E. Burkholder, L. Cronin, *Chem. Soc. Rev.* **2007**, *36*, 105–121.
[2] H. J. Lunk, H. Hartl, *ChemTexts* **2021**, *7*, 1–30.
[3] M. T. Pope, A. Müller, *Angew. Chem. Int. Ed. Engl.* **1991**, *30*, 34–48.
[4] J.-C. Raabe, M. J. Poller, D. Voß, J. Albert, *ChemSusChem* **2023**, *16*, 2013–2015.
[5] I. A. Weinstock, *Chem. Rev.* **1998**, *98*, 113–170.
[6] J.-C. Raabe, J. Albert, M. J. Poller, *Chem. A Eur. J.* **2022**, *28*, 1–12.
[7] J.-C. Raabe, J. Aceituno Cruz, J. Albert, M. J. Poller, *Inorganics* **2023**, *11*, 138.
[8] R. Dehghani, S. Aber, F. Mahdizadeh, *CLEAN: Soil, Air, Water* **2018**, *46*, 1800413.
[9] M. Ammam, *J. Mater. Chem. A* **2013**, *1*.
[10] J. Albert, D. Lüders, A. Bösmann, D. M. M. Guldi, P. Wasserscheid, *16*, 226–237.
[11] J. A. Dias, S. C. L. Dias, E. Caliman, J. Bartis, L. Francesconi, *Inorg. Synth.* **2014**, *36*, 210–217.
[12] D. Voß, S. Ponce, S. Wesinger, B. J. M. Etzold, J. Albert, *RSC Adv.* **2019**, *9*, 29347–29356.
[13] M. J. Poller, S. Bönisch, B. Bertleff, J.-C. Raabe, A. Görling, J. Albert, *Chem. Eng. Sci.* **2022**, *264*, 118143.
[14] I.-M. Mbomekalle, Y. W. Lu, B. Keita, L. Nadjo, *Inorg. Chem. Commun.* **2004**, *7*, 86–90.
[15] D. R. Park, H. Kim, J. C. Jung, S. H. Lee, I. K. Song, *Catal. Commun.* **2008**, *9*, 293–298.
[16] T. Ueda, Y. Nishimoto, R. Saito, M. Ohnishi, J. I. Nambu, *Inorganics* **2015**, *3*, 355–369.
[17] A. M. Khenkin, R. Neumann, *Inorg. Chem.* **2000**, *39*, 3455–3462.
[18] P. Wu, Y. Wang, B. Huang, Z. Xiao, *Nanoscale* **2021**, *13*, 7119–7133.
[19] N. I. Gumerova, A. Rompel, *Nat. Chem. Rev.* **2018**, *2*, 1–20.
[20] I. A. Weinstock, R. E. Schreiber, R. Neumann, *Chem. Rev.* **2018**, *118*, 2680–2717.
[21] D. Mansuy, J.-F. Bartoli, P. Battioni, D. K. Lyon, R. G. Finite, *J. Am. Chem. Soc.* **1991**, *113*, 7222–7226.
[22] A. Modvig, C. Kumpidet, A. Riisager, J. Albert, *Mater.* **2019**, *12*, 2175.
[23] B. Bertleff, J. Claußnitzer, W. Korth, P. Wasserscheid, A. Jess, J. Albert, *ACS Sustainable Chem. Eng.* **2017**, *5*, 4110–4118.
[24] J. Albert, R. Wölfel, A. Bösmann, P. Wasserscheid, *Energy Environ. Sci.* **2012**, *5*, 7956–7962.
[25] F. Lefebvre, *Curr. Catal.* **2017**, *6*, 77–89.
[26] X. López, C. Bo, J. M. Poblet, *J. Am. Chem. Soc.* **2002**, *124*, 12574–12582.
[27] X. López, J. J. Carbó, C. Bo, J. M. Poblet, *Chem. Soc. Rev.* **2012**, *41*, 7537–7571.
[28] B. Keita, L. Nadjo, *J. Mol. Catal. A* **2007**, *262*, 190–215.
[29] H. Zhou, Y. Dong, X. Xin, M. Chi, T. Song, H. Lv, *J. Mater. Chem. A* **2022**, *10*, 19963–19971.
[30] W. Xu, B. Zhou, Q. Wang, G. Xu, N. Li, W. Liu, Z. C. Zhang, *ChemCatChem* **2023**, *15*, e202300522.
[31] M. Li, T. Wang, X. Chen, X. Ma, *Int. J. Hydrogen Energy* **2023**, *48*, 21004–21017.
[32] D. F. Yan, C. Mebrahtu, S. Y. Wang, R. Palkovits, D. F. Yan, C. Mebrahtu, R. Palkovits, S. Y. Wang, *Angew. Chem. Int. Ed.* **2022**, *2023*, e202214333.
[33] R. Francke, R. D. Little, *Chem. Soc. Rev.* **2014**, *43*, 2492–2521.
[34] F. Wang, S. S. Stahl, *Acc. Chem. Res.* **2020**, *53*, 561–574.
[35] A. D. Stergiou, M. D. Symes, *Catal. Today* **2022**, *384–386*, 146–155.
[36] C. Rong, F. C. Anson, F. C. Inorg, *J. Electroanal. Chem. Interfacial Electrochem.* **1994**, *33*, 1517.
[37] J. C. Bart, F. C. Anson, *J. Electroanal. Chem.* **1995**, *390*, 11–19.
[38] M. Sadakane, E. Steckhan, *J. Mol. Catal. A* **1996**, *114*, 221–228.
[39] W. Choi, D. Im, M. S. Park, Y. G. Ryu, S. S. Hwang, Y. S. Kim, H. Kim, S. G. Doo, H. Chang, *Electrochemistry* **2016**, *84*, 882–886.
[40] T. Matsui, E. Morikawa, S. Nakada, T. Okanishi, H. Muroyama, Y. Hirao, T. Takahashi, K. Eguchi, *ACS Appl. Mater. Interfaces* **2016**, *8*, 18119–18125.
[41] M. Kourasi, R. G. A. Wills, A. A. Shah, F. C. Walsh, *Electrochim. Acta* **2014**, *127*, 454–466.
[42] R. Singh, A. A. Shah, A. Potter, B. Clarkson, A. Creeth, C. Downs, F. C. Walsh, *J. Power Sources* **2012**, *201*, 159–163.
[43] L. Z. Abunaeva, E. A. Ruban, M. A. Myachina, P. A. Loktionov, D. E. Verakso, A. A. Pustovalova, M. M. Petrov, D. V. Konev, N. N. Gavrilova, A. E. Antipov, *Russ. J. Electrochem.* **2022**, *58*, 938–945.
[44] R. Neumann, *Inorg. Chem.* **2010**, *49*, 3594–3601.
[45] B. B. Sarma, I. Efremenko, R. Neumann, *J. Am. Chem. Soc.* **2015**, *137*, 5916–5922.
[46] Y. P. Liu, S. F. Zhao, S. X. Guo, A. M. Bond, J. Zhang, G. Zhu, C. L. Hill, Y. V. Geletii, *J. Am. Chem. Soc.* **2016**, *138*, 2617–2628.
[47] M. Bugnola, R. Carmieli, R. Neumann, *ACS Catal.* **2018**, *8*, 3232–3236.
[48] A. D. Stergiou, M. D. Symes, *Cell Reports Phys. Sci.* **2022**, *3*, 100914.
[49] A. D. Stergiou, D. H. Broadhurst, M. D. Symes, *STAR Protoc.* **2022**, *3*, 101817.
[50] A. D. Stergiou, D. H. Broadhurst, M. D. Symes, *ACS Org. Inorg. Au* **2023**, *3*, 51–58.
[51] W. Liu, Y. Cui, X. Du, Z. Zhang, Z. Chao, Y. Deng, *Energy Environ. Sci.* **2016**, *9*, 467–472.
[52] M. Li, T. Wang, M. Zhao, Y. Wang, *Int. J. Hydrogen Energy* **2022**, *47*, 15357–15369.

[53] F. W. S. Lucas, R. G. Grim, S. A. Tacey, C. A. Downes, J. Hasse, A. M. Roman, C. A. Farberow, J. A. Schaidle, A. Holewinski, *ACS Energy Lett.* **2021**, *6*, 1205–1270.
[54] F. Harnisch, U. Schröder, *ChemElectroChem* **2019**, *6*, 4126–4133.
[55] F. J. Holzhäuser, J. B. Mensah, R. Palkovits, *Green Chem.* **2020**, *22*, 286–301.
[56] S. Palkovits, R. Palkovits, *Chem. Ing. Tech.* **2019**, *91*, 699–706.
[57] J. Raabe, T. Esser, F. Jameel, M. Stein, J. Albert, M. J. Poller, *Inorg. Chem. Front.* **2023**, DOI 10.1039/D3QI00937H.
[58] M. J. Poller, S. Bönisch, B. Bertleff, J.-C. Raabe, A. Görling, J. Albert, *Chem. Eng. Sci.* **2022**, *264*, 118143.
[59] D. V. Evtuguin, C. Pascoal Neto, J. Rocha, J. D. Pedrosa de Jesus, *Appl. Catal. A* **1998**, *167*, 123–139.
[60] Z. Tang, W. Deng, Y. Wang, E. Zhu, X. Wan, Q. Zhang, Y. Wang, *ChemSusChem* **2014**, *7*, 1557–1567.
[61] T. Esser, M. Huber, D. Voß, J. Albert, *Chem. Eng. Res. Des.* **2022**, *185*, 37–50.
[62] V. F. Odyakov, E. G. Zhizhina, *Russ. J. Inorg. Chem.* **2009**, *54*, 361–367.
[63] V. F. Odyakov, E. G. Zhizhina, *React. Kinet. Catal. Lett.* **2008**, *95*, 21–28.
[64] V. F. Odyakov, E. G. Zhizhina, R. I. Maksimovskaya, *Appl. Catal. A* **2008**, *342*, 126–130.

Manuscript received: December 12, 2023
Revised manuscript received: January 10, 2024
Accepted manuscript online: January 21, 2024
Version of record online: February 12, 2024